

# TRANSIENT X-RAY SOURCES IN THE MAGELLANIC-TYPE GALAXY NGC 4449

V. JITHESH AND ZHONGXIANG WANG

Shanghai Astronomical Observatory, Chinese Academy of Sciences, 80 Nandan Road, Shanghai 200030, China; jithesh@shao.ac.cn

## ABSTRACT

We report the identification of seven transient X-ray sources in the nearby Magellanic-type galaxy NGC 4449 using the archival multi-epoch X-ray observations conducted with *Chandra*, *XMM-Newton* and *Swift* telescopes over year 2001–2013. Among them, two sources are classified as supersoft X-ray sources (SSSs) because of their soft X-ray color and rest of the sources are X-ray binaries (XRBs). Transient SSSs spectra can be fitted with a blackbody of effective temperature  $\sim 80 - 105$  eV and luminosities were  $\simeq 10^{37} - 10^{38}$  erg s<sup>-1</sup> in 0.3–8 keV. These properties are consistent with the widely accepted model for SSSs, an accreting white dwarf with the steady nuclear burning on its surface, while the SSS emission has also been observed in many post-nova systems. Detailed analysis of one sufficiently bright SSS revealed the strong short-term variability, possibly showing a 2.3 hour periodic modulation, and long-term variability, detectable over 23 years with different X-ray telescopes before year 2003. The X-ray properties of four other transients are consistent with neutron star or black hole binaries in their hard state, while the remaining source is most likely an XRB with a quasi-soft X-ray spectrum. Analysis of archival *Hubble Space Telescope* image data was also conducted, and multiple massive stars were found as possible counterparts. We conclude that the X-ray transient properties in NGC 4449 are similar to those in other Magellanic-type galaxies.

**Keywords:** galaxies: individual (NGC 4449) — X-rays: binaries — X-rays: galaxies — X-rays: general

## 1. INTRODUCTION

NGC 4449 is a Magellanic-type irregular star-forming galaxy, first studied at X-ray wavelengths with the *Einstein* satellite (Fabbiano et al. 1992). The *Einstein* IPC and HRI observations detected three point sources in the galaxy and one of them coincides with an extremely luminous supernova remnant (SNR), previously identified with radio observations (Seaquist & Bignell 1978). The *ROSAT* HRI observations resolved seven luminous X-ray sources in the D<sub>25</sub> region of NGC 4449 and identified an extended emission feature, which is mainly from the unresolved point sources and hot interstellar medium (Vogler & Pietsch 1997). Later, *Chandra* observation (conducted in 2001) has detected 24 X-ray point sources in the optical extend of NGC 4449 and the X-ray point source population has been determined to be dominated by X-ray binaries (XRBs) along with supersoft X-ray sources (SSSs) and SNRs (Summers et al. 2003). It has been found that the X-ray emission from the Magellanic-type galaxies dominantly comes from young population objects and the X-ray sources are spatially associated with the star forming regions (e.g. Stobbart et al. 2006, and references therein). The case of NGC 4449 appears to be consistent with this feature, as the bright XRBs are associated with young star clusters (Rangelov et al. 2011).

The transient X-ray source population has been identified in Magellanic-type galaxies such as the Small and Large Magellanic Clouds (SMC and LMC) and

NGC 55 (Kahabka & Pietsch 1996; Coe et al. 2001; Jithesh & Wang 2016, and references therein). The majority of the transient sources are XRBs, including low-mass and high-mass XRBs. In addition, another important class are SSSs, which contribute approximately 25 – 35% of the total transient population and are the inevitable class of objects in these galaxies.

SSSs are soft X-ray emitting objects, with spectra resembling a blackbody in a temperature range of 20 – 100 eV and X-ray luminosities being in a range of  $10^{35} - 10^{38}$  erg s<sup>-1</sup> (Kahabka & van den Heuvel 1997; Di Stefano et al. 2010, see reviews in). SSSs were first discovered with *Einstein* observatory (Long et al. 1981), and *ROSAT* later discovered more of them in Magellanic Clouds (MCs) and in our Galaxy (Trümper et al. 1991; Greiner et al. 1991; Beuermann et al. 1995), establishing them as an important new class of X-ray objects. Supported by many observational studies, the steady thermonuclear burning of accreted matter on the surface of a white dwarf (WD; van den Heuvel et al. 1992) is the most accepted explanation for SSSs. In addition, SSS emission has also been observed in many nova systems (Oegelman et al. 1984; Henze et al. 2010, 2011, 2014, and references therein). For these cases, a fraction of the hot envelope, most of which has been ejected during a nova explosion, still remains on the surface of a WD (Starrfield et al. 1974) and powers SSS emission. Typical SSSs have little emission above 1 keV, while a companion class of SSSs has been iden-

tified in the external galaxies that have X-ray emission above 1 keV. The latter systems are referred as quasi-soft sources (QSSs) with temperature in a range of 100–350 eV (Di Stefano & Kong 2004). Several SSSs and QSSs identified in the external galaxies (Greiner 2000; Di Stefano & Kong 2003, 2004) are associated with diverse types of objects, which include XRBs with a WD, a neutron star (NS), or a stellar-mass black hole (BH) as the compact object, ultra-luminous SSSs (Kong et al. 2004; Liu & Di Stefano 2008) possibly consisting of an intermediate-mass BH, and SNRs (Orion 2006). The identification studies have further expanded the SSS class.

In this paper, we re-examined the X-ray observations of the Magellanic-type galaxy NGC 4449 to search for the transient X-ray sources. In the following, §2 describes the observations and data reduction processes used. We explain the analysis and results in §3. In §4, we discuss and conclude the properties of the transient X-ray sources found in NGC 4449.

## 2. OBSERVATIONS AND DATA REDUCTION

### 2.1. *Chandra* Observations

We found four sets of archival *Chandra* observations of NGC 4449. The details of the observations are given in Table 1. The *Chandra* observation conducted in 2000 October (ObsID: 938) pointed at a target which is  $\sim 17$  arcmin away from NGC 4449 and the sources considered in this analysis were not covered by this observation. Hence we did not include this data in the analysis. The data from the other three observations were taken with the Advanced CCD Imaging Spectrometer Spectroscopy Array (ACIS-S), and NGC 4449 was positioned on the back-illuminated S3 chip. We processed the data using the *Chandra* Interactive Analysis of Observation (CIAO) software (version 4.6) and *Chandra* Calibration Data Base (CALDB) version 4.6.1.1. The source detection routine was carried out in the ACIS data over the 0.3–8 keV energy band. We used CIAO’s Mexican-hat wavelet source detection routine, WAVDETECT (Freeman et al. 2002), to detect the X-ray sources in NGC 4449. After the production of an exposure map, we ran the WAVDETECT tool with wavelet scales of 1.4, 2, 4, 8 and 16 pixels and a detection threshold of  $5 \times 10^{-7}$ .

### 2.2. *XMM-Newton* and *Swift* Observations

NGC 4449 was observed twice with the *XMM-Newton* telescope (Jansen et al. 2001). The European Photon Imaging Camera (EPIC) PN (Strüder et al. 2001) and metal oxide semiconductor (MOS; Turner et al. 2001) camera were operated in the full frame mode and the thin filter was used in both observations. The details of the *XMM-Newton* observations of NGC 4449 are given in Table 1. The data sets were processed with the Science Analysis Software (SAS version 14.0). We processed PN and MOS data using EPCHAIN and EMCHAIN to produce calibrated photon event files, and used unflagged single and double pixel events with PATTERN 0–4 and

**Table 1.** Observation log

| Observatory    | Data  | ObsID | Date        | Exposure <sup>a</sup> |
|----------------|-------|-------|-------------|-----------------------|
| <i>Chandra</i> | C0    | 938   | 2000 Oct 04 | 5.7                   |
|                | C1    | 2031  | 2001 Feb 04 | 26.9                  |
|                | C2    | 10125 | 2009 Mar 04 | 15.1                  |
|                | C3    | 10875 | 2009 Mar 07 | 60.2                  |
| <i>XMM-</i>    | XMM1  | K601  | 2002 May 25 | 23.9                  |
| <i>Newton</i>  | XMM2  | K701  | 2002 Jun 02 | 15.9                  |
| <i>Swift</i>   | S1    | L3001 | 2007 Mar 27 | 4.7                   |
|                | S2    | M1007 | 2013 Dec 06 | 4.9                   |
| <i>HST</i>     | POS-A | 10585 | 2005 Nov 10 | 3.7 (F435W)           |
|                |       |       |             | 2.5 (F555W)           |
|                |       |       |             | 2.1 (F814W)           |
|                | POS-B | 10585 | 2005 Nov 11 | 3.5 (F435W)           |
|                |       |       |             | 2.5 (F555W)           |
|                |       |       |             | 2.1 (F814W)           |
|                | POS-C | 10585 | 2005 Nov 17 | 0.5 (F814W)           |

NOTE—<sup>a</sup>Exposure time is in unit of kilo seconds. The prefix K, L and M denote 0112521, 0003587 and 0008226 respectively.

0–12 to filter the processed PN and MOS events respectively. To exclude particle flaring background, we created a Good Time Interval (GTI) file above 10 keV for the full field using the task TABGTIGEN. The general cut-off value was  $\text{RATE} < 0.4 \text{ count s}^{-1}$ . However for the XMM1 observation (Table 1), which has a high particle background, we used much higher cut-off value ( $\text{RATE} < 4 \text{ count s}^{-1}$ ) for the filtering. As a result, we obtained  $\sim 1$  ks usable data from this observation. To detect the X-ray sources from *XMM-Newton* observations, we ran the source detection routine available in SAS, EDETECT.CHAIN, using the standard parameters for EPIC-PN data over the entire energy band as well as the 0.3–1 keV, 1–2 keV, and 2–8 keV bands.

In addition, we checked the long-exposure ( $> 4$  ks; see Table 1) observations of the target field conducted with the *Swift* X-ray Telescope (XRT; Burrows et al. 2005) for possible detection of transient sources found in the *Chandra* and *XMM-Newton* observations. However, none of the transient sources were detected in the *Swift* XRT observations.

### 2.3. *Hubble Space Telescope* Observations

We searched for possible optical counterparts of transient X-ray sources in the *Hubble Space Telescope* (*HST*) observations. We used image data taken with the Wide Field Channel (WFC) camera of the Advanced Camera for Surveys (ACS), which were downloaded from the Hubble Legacy Archive<sup>1</sup> (HLA). The images were generated from the individual flat-fielded exposures using the

<sup>1</sup> <http://hla.stsci.edu/>

**Table 2.** Transient X-ray sources in NGC 4449

| Src<br>No. | ObsID    | Catalog<br>No. & Ref.           | R.A.<br>(h:m:s) | Decl.<br>(° :′ :″) | SC               | HC               | Class |
|------------|----------|---------------------------------|-----------------|--------------------|------------------|------------------|-------|
| TSS1       | C1       | X3(AV97), 14(LKS03)             | 12:28:10.94     | +44:03:38.18       | $-0.99 \pm 0.01$ | –                | SSS   |
|            | XMM1-PN  |                                 |                 |                    | $-0.44 \pm 0.09$ | –                | SSS   |
|            | XMM1-MOS |                                 |                 |                    | $-1.18 \pm 0.34$ | –                | SSS   |
|            | XMM2-PN  |                                 |                 |                    | $-0.99 \pm 0.02$ | $0.33 \pm 0.53$  | SSS   |
|            | XMM2-MOS |                                 |                 |                    | $-0.96 \pm 0.06$ | $-0.99 \pm 1.99$ | SSS   |
| TSS2       | C1       | 28(LKS03), P18(JO05), X19(BR11) | 12:28:19.03     | +44:05:44.59       | $-0.96 \pm 0.04$ | –                | SSS   |
| T3         | C1       | 6(LKS03), X13(BR11)             | 12:28:06.88     | +44:05:28.27       | $0.25 \pm 0.08$  | $-0.67 \pm 0.20$ | XRB   |
| T4         | C1       | 2(LKS03), X8(BR11)              | 12:28:00.73     | +44:04:32.24       | $0.30 \pm 0.12$  | $0.03 \pm 0.01$  | XRB   |
| T5         | C3       | X43(BR11)                       | 12:28:20.03     | +44:06:21.36       | $1.00 \pm 0.44$  | $0.14 \pm 0.04$  | ABS   |
| T6         | C3       | X44(BR11)                       | 12:28:13.25     | +44:06:46.05       | $0.09 \pm 0.06$  | $0.29 \pm 0.10$  | XRB   |
| T7         | C3       | X46(BR11)                       | 12:28:09.71     | +44:05:19.35       | $-0.44 \pm 0.08$ | $-0.67 \pm 0.24$ | SNR   |

NOTE—(1) Source number used in this paper; (2) observation ID in which the source was detected; (3) source identification number from previous studies, AV97=Vogler & Pietsch (1997), LKS03=Summers et al. (2003), JO05=Ott et al. (2005), BR11=Rangelov et al. (2011); (4)-(5) right ascension (R.A.) and declination (Decl.) of each source (J2000.0); (6)-(7) X-ray colors derived from the count rate (See §3.1); (8) source class according to the classification scheme of Kilgard et al. (2005) and Jenkins et al. (2005).

IRAF task MULTIDRIZZLE<sup>2</sup>. Three sets of the images covering NGC 4449 (POS-A, POS-B and POS-C) were taken with the F435W (*B*), F555W (*V*), and F814W (*I*) filters (see Table 1 for details).

### 3. ANALYSIS AND RESULTS

#### 3.1. Transients and their X-ray Colors

To search for transient sources, we mainly used the long-separated and long-exposure *Chandra* observations (C1 and C3), while the other *Chandra* and *XMM-Newton* observations (C2, XMM1, and XMM2) were used for checking the luminous fast transients and follow-up studies. We detected 24 and 23 X-ray sources in the D<sub>25</sub> region of the galaxy in the 2001 (C1) and 2009 (C3) *Chandra* observations respectively. Four sources detected in C1 did not appear in C3, and on the other hand three sources in C1 were brighter in C3. However, no other transient events were detected in the short-exposure observations. Thus, we identified seven transient X-ray sources in NGC 4449 (See Table 2). We ran the source detection algorithm again on the soft (*S*: 0.3–1 keV), medium (*M*: 1–2 keV), and hard (*H*: 2–8 keV) images and the transient sources were detected in at least one of the three energy bands.

The count rates of the transient sources in the three energy bands were obtained, and we calculated two X-ray colors, defined as,  $SC = (M - S)/(M + S)$ ,  $HC = (H - M)/(H + M)$ . To understand the source class of the transient sources, we compared the X-ray colors of the sources with the color classification scheme provided in Kilgard et al. (2005) and Jenkins et al. (2005) for *Chandra* and *XMM-Newton* sources respectively. For the *XMM-Newton* observations, we defined the 0.3–1 keV,

1–2 keV, and 2–6 keV energy band as *S*, *M*, and *H*, respectively. The transient source positions, X-ray colors, and their respective source classes are given in Table 2. Out of seven sources, three of them (T3, T4 and T6) are in the XRB class, one source each in the absorbed (ABS) and SNR category (T5 and T7 respectively), and the rest of the two sources, named as TSS1 and TSS2, belong to the SSS class. Earlier studies (Vogler & Pietsch 1997; Summers et al. 2003; Ott et al. 2005; Rangelov et al. 2011) also identified these sources in their respective classes. Here we further classified them as the transient X-ray sources in NGC 4449. Among them, T7 has a color consistent with SNR, but the transient behavior rules out the SNR nature of this source. In the following sections, we describe their detailed properties we obtained.

#### 3.2. TSS1

TSS1 is one of the brightest sources in NGC 4449 and was also detected by previous X-ray telescopes (*Einstein* and *ROSAT*; Fabbiano et al. 1992; Vogler & Pietsch 1997). The source was detected in the C1 observation (Summers et al. 2003) but was not in the C2 and C3 observations. For the detection, we extracted the source and background events within a circular region with a radius of 5 arcsec. Using the CIAO SPEXTRACT tool, we obtained the source and background spectra along with the ancillary response file (ARF) and redistribution matrix file (RMF). The source spectrum was grouped with a minimum of 20 counts per bin and the spectral analysis was performed in the 0.3–8 keV energy range with XSPEC version 12.8.1g (Arnaud 1996) available in the HEASOFT (version 6.15.1). TSS1 has a few tens of spectral counts below 0.3 keV energy. Since the calibration of the spectral response of the instruments is less certain at the low energies, we did not include these

<sup>2</sup> [http://www.stsci.edu/hst/HST\\_overview/documents/multidrizzle](http://www.stsci.edu/hst/HST_overview/documents/multidrizzle)

photons in the spectral analysis. However, they were included in the light curve analysis (see §3.2.1). In the undetected observations, we computed the upper limits on the count rate (90% confidence level) using the APRATES task in CIAO.

In both *XMM-Newton* observations, the source was detected and we used a circular region with a radius of 18 arcsec for both source and background event extraction. For the EPIC-PN and MOS data, the source and background spectra along with associated files (ARF and RMF) were extracted using the SAS tool ESPECGET, and fitted simultaneously.

We used a blackbody (BBODY) model to fit the spectra, which was modified by the Galactic absorption,  $N_{\text{H,Gal}} = 1.61 \times 10^{20} \text{ cm}^{-2}$  (Kalberla et al. 2005). For all the spectra, the absorption-corrected fluxes were derived in the 0.3 – 8 keV energy band using the convolution model CFLUX available in XSPEC, and the luminosities were calculated by assuming a distance of 2.93 Mpc (Karachentsev & Drozdovsky 1998). All errors quoted were computed at a 90% confidence level. The best-fit spectral parameters are given in Table 3. We tested to add another absorption component (tbabs), which was considered to account for the local absorption within the galaxy and/or material around the source. The additional absorption component did not improve the spectral fit compared to the absorbed blackbody model and the absorption values were not well constrained,  $N_{\text{H}} < 10.4 \times 10^{20} \text{ cm}^{-2}$ .

### 3.2.1. Light Curve and Long-term Variability

We investigated the source variability using the results from the *Chandra* and *XMM-Newton* observations. We derived the binned and background subtracted light curve using CIAO task DMEXTRACT. For the light curve, the extraction regions were the same as those for obtaining the spectra. Since low-energy emission from the source is dominant, we only included the events in the 0.2 – 2 keV energy band in the light curve. The light curve of TSS1 obtained from the C1 observation is shown in Figure 1. There is clear variability seen in the light curve. We tested to fit a sinusoid to the light curve, which gave a reduced  $\chi^2$  of 1.2 for 42 degrees of freedom (d.o.f). While the low  $\chi^2$  value is due to the large uncertainties of the data points, a period of  $139 \pm 4$  min was found. This period is also marginally consistent with a peak ( $\sim 160$  min) obtained from the power spectral analysis (using powspec task).

In the *XMM-Newton* observations, the source and background light curves were extracted from the cleaned event files and corrected using the SAS task EPICLCCORR. The quality and length of the light curve do not allow us to confirm the periodic variability seen in the *Chandra* observation. However, we investigated the short-term X-ray variability by performing a Kolmogorov-Smirnov (K-S) test on the light curve. From the K-S test, we found that the source showed a strong X-ray variability in short time scale (600 s) at a confidence level of  $> 99\%$ .

**Table 3.** Spectral parameters for transient X-ray sources in NGC 4449

| Src  | ObsID | kT/ $\Gamma$           | log $L_{\text{X}}$      | $\chi^2/\text{d.o.f}$ | $G$  |
|------|-------|------------------------|-------------------------|-----------------------|------|
| No.  |       |                        | erg s $^{-1}$           |                       |      |
| TSS1 | C1    | $104.9^{+10.3}_{-8.9}$ | $37.87^{+0.04}_{-0.04}$ | 9.3/12                | 0.68 |
|      | XMM1  | $89.3^{+22.0}_{-20.8}$ | $38.11^{+0.14}_{-0.19}$ | 26.3/19               | 0.12 |
|      | XMM2  | $86.0^{+6.5}_{-6.1}$   | $37.85^{+0.04}_{-0.05}$ | 26.6/21               | 0.19 |
|      | C2    | ...                    | $< 36.51$               | ...                   | ...  |
|      | C3    | ...                    | $< 36.25$               | ...                   | ...  |
| TSS2 | C1    | $76.1^{+16.0}_{-13.7}$ | $36.92^{+0.13}_{-0.15}$ | 9.1/7(C)              | 46%  |
|      | XMM1  | ...                    | $< 37.24$               | ...                   | ...  |
|      | XMM2  | ...                    | $< 36.70$               | ...                   | ...  |
|      | C2    | ...                    | $< 36.37$               | ...                   | ...  |
|      | C3    | ...                    | $< 36.05$               | ...                   | ...  |
| T3   | C1    | $1.36^{+0.95}_{-1.35}$ | $36.71^{+0.29}_{-0.32}$ | 3.9/3(C)              | 26%  |
|      | C2    | ...                    | $< 36.95$               | ...                   | ...  |
|      | C3    | ...                    | $< 36.59$               | ...                   | ...  |
| T4   | C1    | $< 2.35$               | $37.09^{+1.29}_{-0.80}$ | 0.2/2(C)              | 1%   |
|      | C2    | ...                    | $< 36.21$               | ...                   | ...  |
|      | C3    | ...                    | $< 36.28$               | ...                   | ...  |
| T5   | C1    | ...                    | $< 36.74$               | ...                   | ...  |
|      | C2    | ...                    | $< 36.63$               | ...                   | ...  |
|      | C3    | $0.38^{+0.73}_{-0.80}$ | $36.89^{+0.27}_{-0.27}$ | 2.3/4(C)              | 10%  |
| T6   | C1    | ...                    | $< 36.85$               | ...                   | ...  |
|      | C2    | ...                    | $< 36.97$               | ...                   | ...  |
|      | C3    | $0.88^{+0.93}_{-0.80}$ | $36.86^{+0.21}_{-0.21}$ | 8.2/4(C)              | 56%  |
| T7   | C1    | ...                    | $< 36.59$               | ...                   | ...  |
|      | C2    | ...                    | $< 36.82$               | ...                   | ...  |
|      | C3    | $3.65^{+1.03}_{-0.96}$ | $36.94^{+0.38}_{-0.27}$ | 12.5/5(C)             | 70%  |

NOTE—The absorption was fixed at Galactic value in all cases. (1) Source number; (2) observation ID used in each fit; (3) blackbody temperature in eV for TSS1 and TSS2 and photon index for rest of the sources; (4) absorption-corrected X-ray luminosity in the 0.3 – 8 keV energy band; (5) the  $\chi^2/\text{d.o.f}$  value for the model and ‘C’ in the bracket indicates that C-statistics is used for spectral modeling; (6) goodness-of-fit (Null hypothesis probability for  $\chi^2$  statistics and “Goodness” value when using C-Statistics).

We also studied the long-term variability of TSS1 using *Chandra*, *XMM-Newton* and *Swift* observations. The baseline of the long-term light curve was extended by adding the data points from *Einstein* HRI, *ROSAT* PSPC, and *ROSAT* HRI observations. NGC 4449 was observed with HRI onboard *Einstein* observatory in December 1979 (Fabbiano et al. 1992) and TSS1 was identified as one of the three X-ray sources in the galaxy (HEASARC HRIEXO catalog<sup>3</sup>). The source was bright during the *Einstein* observation with a count rate of  $(1.1 \pm 0.3) \times 10^{-3} \text{ count s}^{-1}$ . The *ROSAT* PSPC and HRI observations were conducted in November 1991 and December 1994 respectively (Vogler & Pietsch 1997),

<sup>3</sup> <http://heasarc.gsfc.nasa.gov/W3Browse/einstein/hriexo.html>



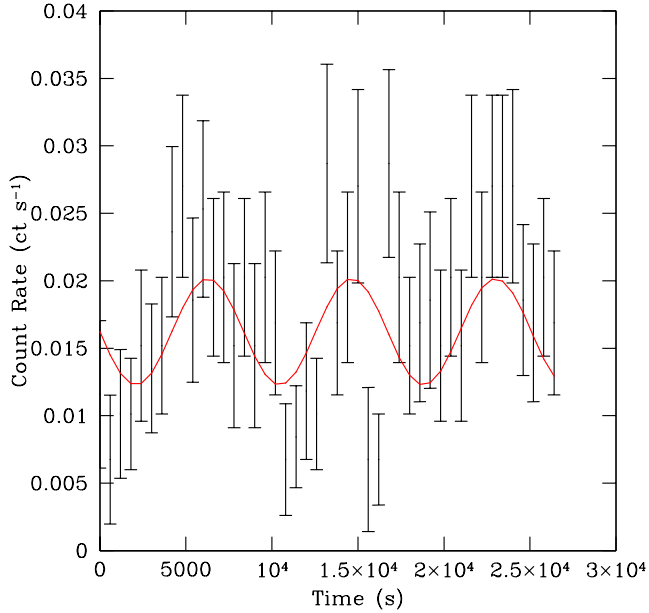


**Figure 1.** Background subtracted ACIS-S (0.2 – 2 keV) light curve of TSS1 with a bin size of 600 s. A sinusoidal modulation with period of 139 min fitted to the data is also shown.

and TSS1 (X3 in *ROSAT*) was detected in both observations with count rates of  $(3.3 \pm 1.1) \times 10^{-3}$  and  $(27.3 \pm 4.4) \times 10^{-4}$  count  $s^{-1}$  respectively. In the available long-exposure *Swift* XRT observations, TSS1 was not detected and we derived the upper limits of the count rates using the `uplimit` command in XIMAGE. We converted the *Einstein*, *ROSAT* and *Swift* XRT count rates into fluxes in the 0.3 – 8 keV energy band using the webPIMMS<sup>4</sup> by assuming an absorbed blackbody model. Figure 2 shows the long-term light curve of TSS1 over  $\sim 34$  years. The source appeared to have a constant X-ray luminosity ( $\sim 10^{38}$  erg  $s^{-1}$ ) over a period of  $\sim 23$  years, although the ill-sampled observations could have missed the intervals of stronger or weaker states of the source. The source then became undetectable in the *Swift* (conducted in 2007) and two *Chandra* observations conducted in 2009, which indicate a flux change of at least two orders of magnitude. We estimated the duty cycle of TSS1 as the ratio of the time spent in “on-state” (observations where the source was detected) to the total time in both “on-state” and “off-state” (the non-detection observations). Assuming that TSS1 was in the on-state during 1979 – 2002 period, the duty cycle is  $\sim 0.6$ .

### 3.3. TSS2

TSS2 (CXOJ122819.03+440544.59) was detected only in the C1 observation. We extracted the source and background events from a circular region with a ra-

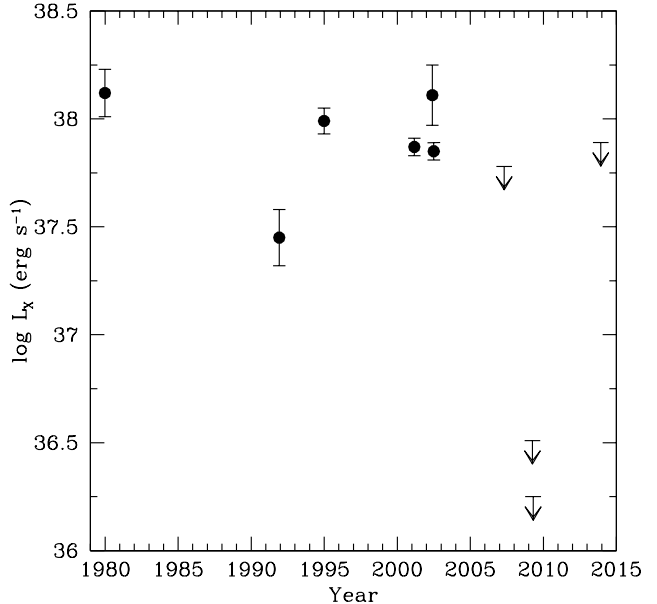


**Figure 2.** Long-term 0.3 – 8 keV light curve of TSS1 based on *Einstein*, *ROSAT*, *Chandra*, *XMM-Newton* and *Swift* observations. See the text for details.

dius of 3 arcsec. The extracted spectrum was fitted with an absorbed blackbody model, and the best-fit spectral parameters are  $kT = 76.1^{+16.0}_{-13.7}$  eV with  $L_X = (8.3^{+2.9}_{-2.4}) \times 10^{36}$  erg  $s^{-1}$  (see also Table 3). Since TSS2 has limited net spectral counts, we adopted Cash-Statistics (Cash 1979) for the spectral modeling and the quality of the fit was obtained by performing 5000 Monte Carlo simulations using `goodness` task. The source was then not detected in the XMM1, XMM2, C2 and C3 observations. We derived the upper limits on the count rate (90% confidence level) from a circular region of 10 arcsec radius using the SAS task `ERECTIONANALYSE` for the *XMM-Newton* observations. The upper limits were converted into fluxes by assuming the best-fit model parameters obtained from the C1 observation. The upper limits are provided in Table 3. We extracted the background-subtracted light curve of TSS2, binned with 100 s and 600 s intervals, and performed the K-S test to investigate the variability. However, the limited net counts do not allow us to obtain any meaningful results from the light curves.

### 3.4. Other Transient Sources

The five transient sources (T3, T4, T5, T6 and T7) were detected either in C1 or C3 observations. We extracted the spectra and upper limits of these sources using CIAO tools. Since these sources have limited net counts, a detailed analysis is not possible. We tested to fit their spectra with absorbed power law (PL) model and the results are presented in Table 3. This model gives a reasonable fit to all sources, except T7. T7 has a steep PL index ( $\sim 3.7$ ) from the absorbed PL fit. Thus, we tested BBODY model for T7 and this

<sup>4</sup> <http://heasarc.gsfc.nasa.gov/cgi-bin/Tools/w3pimms/w3pimms.pl>

model marginally improved the spectral fit (in terms of goodness-of-fit) over the PL model. The spectral parameters for BBODY model are  $kT = 177.4^{+45.6}_{-33.2}$  eV,  $L_X = (4.2^{+1.8}_{-1.4}) \times 10^{36}$  erg s $^{-1}$  with  $\chi^2/\text{d.o.f} = 9.5/5$ . In the *XMM-Newton* observations, these sources were not well resolved and undetected. In some cases, they were located in the edges of the CCD and contaminated by other nearby sources. Hence, the *XMM-Newton* upper limits of these sources were not obtained. The deep *Chandra* observations provided the upper limits in all cases.

### 3.5. Search for Possible Optical Counterparts

The possible optical counterparts of the seven transient sources were searched in the *BVI* band images obtained with *HST* ACS. We performed the astrometric calibration of the X-ray and optical images using the stars from the U.S. Naval Observatory catalog (USNO-B; Monet et al. 2003). The plate solution was computed using the IRAF tool *ccmap* and the root mean square (rms) residuals were typically less than a few tenths to hundredths of an arcsecond in both R.A. and decl. The total alignment errors were computed by summing X-ray and optical rms residuals in quadrature and applied to the coordinates of each X-ray source. The NGC 4449 POS-A and POS-B pointings covered six transients. While TSS1 is outside of the field of view of the both observations, the POS-C observation covered TSS1 in its field of view (close to the edge of the CCD). We identified the optical sources in each filter using IRAF DAOFIND task. Most of the transient source regions are crowded (see Figure 3) and multiple optical sources were identified in the 0.6 arcsec radius error circle (90% uncertainty of the *Chandra* X-ray absolute positions for ACIS-S<sup>5</sup>). The magnitudes of these optical sources were computed using the DAOPHOT package in IRAF. We also calculated the logarithmic X-ray-to-optical flux ratio  $\log(f_x/f_o)$ , where  $f_x$  and  $f_o$  are the 0.3–8 keV X-ray flux and the F555W flux respectively. For TSS1, we used the optical flux from the F814W band instead. The absolute magnitude, color, X-ray-to-optical flux ratio, and the likely class of each source are given in Table 4.

X-ray-to-optical flux ratios can be used to identify the class of the X-ray sources. The flux ratios of stars have wide-range values of typically  $\log(f_x/f_o) < 0$ , while those of the active galactic nuclei (AGNs) and BL Lac objects are  $> 1$  (Maccacaro et al. 1982; Stocke et al. 1991). In SMC, the X-ray pulsars and high-mass X-ray binaries (HMXBs) have a flux ratio of  $\lesssim 1$  with  $B - V \lesssim 0$  (McGowan et al. 2008). All the optical sources, except one source in the TSS1 error circle, have the flux ratio  $< 1$ . Thus, they are consistent with X-ray pulsars or HMXBs. In SMC, the Be-XRBs dominate the population of HMXBs with  $M_V \sim -2$  to  $-5$

**Table 4.** Possible optical counterparts of transient X-ray sources in NGC 4449

| Src  | Opt | $M$       | Range of<br>( $B - V$ ) | Range of<br>( $V - I$ ) | log<br>( $f_x/f_o$ ) |
|------|-----|-----------|-------------------------|-------------------------|----------------------|
| TSS1 | a   | $-3.3(I)$ | ...                     | ...                     | $[0.80, 1.43](H/A?)$ |
|      | b   | $-1.7(I)$ |                         |                         |                      |
| TSS2 | a   | $-1.5(V)$ | $[-0.50, 0.86]$         | $[-0.29, 0.64]$         | $[0.31, 0.55](H)$    |
|      | b   | $-1.4(V)$ |                         |                         |                      |
|      | c   | $-0.9(V)$ |                         |                         |                      |
| T3   | a   | $-2.4(V)$ | $[0.54, 1.51]$          | $[1.13, 1.21]$          | $[-0.27, -0.13](H)$  |
|      | b   | $-2.1(V)$ |                         |                         |                      |
| T4   | a   | $-0.9(V)$ | $[0.78, 1.54]$          | $[0.51, 0.98]$          | $[0.72, 0.86](H)$    |
|      | b   | $-0.5(V)$ |                         |                         |                      |
| T5   | a   | $-3.3(V)$ | $[-0.15, 0.01]$         | $[-0.50, -0.14]$        | $[-0.45, 0.01](H)$   |
|      | b   | $-2.6(V)$ |                         |                         |                      |
|      | c   | $-2.5(V)$ |                         |                         |                      |
| T6   | a   | $-2.7(V)$ | $[0.27, 1.33]$          | $[0.07, 1.78]$          | $[-0.23, 0.53](H)$   |
|      | b   | $-1.5(V)$ |                         |                         |                      |
|      | c   | $-0.8(V)$ |                         |                         |                      |
| T7   | a   | $-5.7(V)$ | $[-0.50, 1.11]$         | $[-0.81, 1.88]$         | $[-1.65, -0.23](H)$  |
|      | b   | $-4.1(V)$ |                         |                         |                      |
|      | c   | $-3.6(V)$ |                         |                         |                      |

NOTE—(1) Source number; (2) optical sources marked in Figure 3; (3) the absolute magnitude of the marked optical sources and the corresponding filter is given in bracket; (4)-(5) range of  $B - V$  and  $V - I$  colors of the optical sources; (6) range of logarithmic X-ray-to-optical flux ratio and the likely class (H = HMXBs and A = AGN) is given in bracket.

(McBride et al. 2008). At the distance of NGC 4449, these absolute magnitudes correspond to  $m_V \approx 25 - 22$ , and the majority of the optical sources in the error circles are consistent with this range. Considering some of them as possible counterparts, they would thus likely be Be-HMXBs. However, the colors of these optical sources are in the range of  $B - V \sim [-0.5, 1.5]$  and  $V - I \sim [-0.8, 1.9]$ , which are broadly consistent with blue/red bright giants or supergiants. Among the transient sources, T7 (X46 in Rangelov et al. 2011) was identified to be associated with a young star cluster of age  $\sim 5$  Myr. Our analysis also identified the star cluster in the T7 region (source “a”), although there are other less bright sources in the region.

## 4. DISCUSSION

Using archival *Chandra*, *XMM-Newton*, and *Swift* observations, we studied the transient X-ray sources in the Magellanic-type galaxy NGC 4449. We found seven transient sources, two of which are classified as SSSs because of their extreme soft X-ray colors, four are in the XRB class (T7 is considered as an XRB), and one source belongs to the absorbed class. These sources were also identified in the previous studies, but our analysis further classified them as transient X-ray sources in NGC 4449.

<sup>5</sup> <http://cxc.harvard.edu/cal/ASPECT/celmon/index.html>

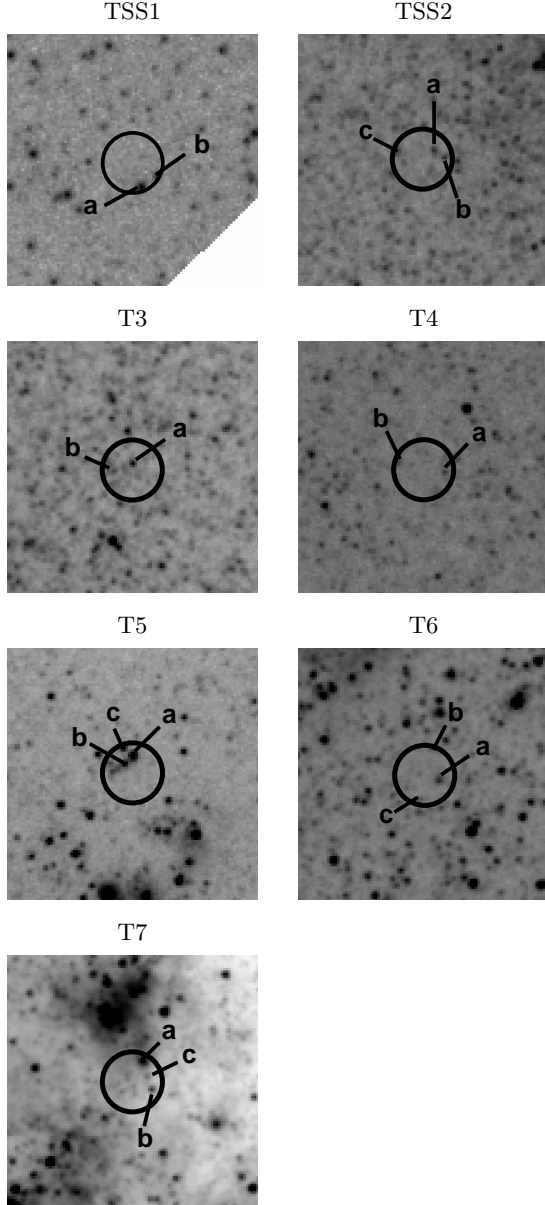


**Figure 3.** Optical *HST* images for transient X-ray sources in NGC 4449. The box size is  $5 \times 5$  arcsec. North is up, and east is to the left. The radius of the black circle is 0.6 arcsec. The three brightest objects inside the error circle were labeled as “a”, “b” and “c” (or “a” and “b” when there are only two sources) and their absolute magnitudes are given in Table 4.

#### 4.1. Transient SSSs

The deep sensitivities of *Chandra* observations have indicated that the transient SSSs changed their fluxes by at least 1–2 orders of magnitude and become undetectable in the later observations. The spectra of the transient SSSs TSS1 and TSS2 were better described by an absorbed blackbody model, with the temperature ranging from  $\sim 75$  to  $105$  eV. The X-ray luminosity in the  $0.3 - 8$  keV band was  $\sim 10^{38}$  erg  $s^{-1}$  for TSS1, while TSS2 was less luminous compared to TSS1, with  $L_X \sim 10^{37}$  erg  $s^{-1}$ . The effective

blackbody temperatures and luminosities inferred from the X-ray spectra are consistent with the characteristics of steady nuclear burning on  $\sim 0.6 - 1.4 M_{\odot}$  WDs (van den Heuvel et al. 1992; Nomoto et al. 2007). Apart from this, the transient SSSs displayed short-term X-ray variability in the X-ray observations, which supports the binary nature of the systems. The supersoft emission at lower luminosities can be from cooling isolated NS, Galactic stars, cataclysmic variables (CVs), and AGN (Kahabka & van den Heuvel 2006; Kahabka & Haberl 2006; Kahabka et al. 2008). However, the transient behavior, binary nature, and high X-ray luminosity help to rule out the isolated stars, CVs, and AGN as the possible class for the transient SSSs. The X-ray luminosities inferred from *Chandra* and *XMM-Newton* observations are also consistent with those of Be/NS X-ray binaries (Reig 2011). Be/NS systems dominantly emit hard X-ray radiation, but sometimes a soft excess is also expected along with hard X-ray emission (Hickox et al. 2004). For our cases, only supersoft X-ray emission was seen, indicating that they unlikely are Be/NS binaries. Thus, the transient SSSs may belong to the X-ray binary class (HMXB) with a WD as the compact object and supersoft X-ray emission is due to the stable nuclear burning on the WD surface. This possibility is supported by the results from the optical analysis of the images of the source fields.

In TSS1, we found possible periodic variations from one *Chandra* observation with a timescale of  $\sim 2.3$  h. Considering the timescale as the orbital period, it is actually consistent with those of the luminous SSSs in our Galaxy, SMC and LMC, derived from photometric variations (Kahabka & van den Heuvel 1997). Moreover, the post-nova phase of classical, recurrent or symbiotic nova is identified in several SSSs and their orbital periods are in the range of  $\sim 85$  min to  $5.3$  h (Kahabka & van den Heuvel 2006). However with the available data, we covered only a few cycles of the possible modulation, and it is thus hard to clarify the periodic nature of the variability. In order to confirm it, future sufficiently long X-ray observations are required once it is back to be bright again.

TSS1 was detected with *Einstein*, *ROSAT*, *Chandra*, and *XMM-Newton* observations. Despite of the ill-sampled observations, the source was possibly active for  $\sim 23$  years and the X-ray luminosity was nearly constant around  $\sim 10^{38}$  erg  $s^{-1}$ . Possibly after year 2002 or 2007 the source became undetectable, even in deep *Chandra* observations. These results suggest that TSS1 may belong to a sub-class of SSSs with a small orbital period ( $\sim 1 - 5$  h), similar to classical novae, but with long SSS phase ( $> 10$  years). Such characteristics favor a slightly low mass WD ( $\sim 0.6 - 0.8 M_{\odot}$ ) in the system (Hachisu et al. 2008; Kato 2010). Moreover, TSS1 has seemingly shown a decreasing trend in temperature ( $\sim 105$  to  $86$  eV), which may provide the further support for a lower mass WD system (Kahabka et al. 2008). TSS2 exhibited short supersoft X-ray phase (detected

only in 2001 observation), indicative of a massive WD system (Kato 2010).

The non-detection of X-ray emission from the transient SSSs can be due to the exhaustion of nuclear burning on the WD surface. Such scenario is possible for post-nova SSSs, if their accretion rate is too low to sustain the steady nuclear surface burning. A nova explosion (either classical or recurrent) in future from transient SSSs can re-ignite the nuclear burning, which is followed with another bright supersoft X-ray phase (Sturm et al. 2012). This feature gives importance to the future observations of the source field.

The post-nova X-ray emission has been observed in many SSSs, for example the first discovered SSS Nova Muscae 1983 (GQ Mus; Oegelman et al. 1984). GQ Mus has been observed to emit in soft X-ray for a long period ( $\sim 10$  years; Oegelman et al. 1993) after outburst and later turned off due to the complete consumption of the residual material (Shanley et al. 1995). The nova explosion and SSSs connection has been well established by the frequent observations of the central region of M31 (Henze et al. 2010, 2011, 2014). Using the dedicated observations in 2006 - 2012, a sample of 79 novae with SSS counterparts in M31 has been identified and the duration of their SSS phase was determined. Among the novae, M31N 1996-08b and M31N 1997-11a were active for more than a decade ( $\sim 13.8$  and  $\sim 11.5$  yr respectively) in X-rays after their optical discovery (Henze et al. 2011) and became undetectable in the later observations (Henze et al. 2014). Since the outburst history is not known for TSS1 and TSS2, the turn-off time of these sources can be estimated as  $> 25.9$  and  $> 0.7$  yr respectively (by assuming the mid point between the *XMM-Newton* and *Chandra* observations). TSS1 was detected with most of the X-ray observatories (see §3.2.1), i.e., active for  $\sim 23$  yr, thus one can argue that TSS1 has the longest SSS phase known so far followed by the Galactic nova V723 Cas (Ness et al. 2008; Schwarz et al. 2011), which has the SSS turn-off time  $\sim 18$ – $19$  yr (Ness et al. 2015).

Some of the classical SSSs exhibited the X-ray off-state for a short timescale. For example, the prototypical SSS CAL83 underwent eight temporary X-ray off-states during 1996 – 2008 (see Kahabka 1998; Greiner & Di Stefano 2002; Rajoelimanana et al. 2013, and references therein). All the X-ray off-states occurred during optical high states (Rajoelimanana et al. 2013) and their duration is less than 120 d (Kahabka 1998). The most likely explanation for the observed X-ray and optical variability is the expansion/contraction of WD's photosphere (Greiner & Di Stefano 2002). In the case of TSS1 and TSS2, one can assume that the X-rays turned off after year 2002 and 2001 (the last detected X-ray observation) respectively, but they were not caught in its normal X-ray on-state in any of the later observations. The available observations could have missed the X-ray on-state and such variability can be confirmed by the continuous monitoring observations in X-ray and opti-

cal wavelength.

#### 4.2. NS and BH X-ray Transients

Four less-luminous transient sources (T3, T4, T5 and T6) were fitted with an absorbed PL with  $\Gamma \sim 0.4 - 2.4$  and their luminosities are  $\leq 10\%$  Eddington luminosity ( $L_{Edd}$ ) for NS and BH primaries. The NS or BH XRBs exhibit the hard-state (Remillard & McClintock 2006) spectrum only at luminosities  $\leq 10\%L_{Edd}$  (Gladstone et al. 2007). Thus, the spectral properties indicate that these sources are possibly NS or BH XRBs at the hard state in NGC 4449. Source T7 had a steep PL index from the spectral fit, which indicates its soft emission. The spectral modeling with blackbody model provided a temperature of  $\sim 180$  eV, which is higher than that of the typical SSSs, but consistent with QSSs (Di Stefano & Kong 2004). QSSs in external galaxies are associated with SNRs and NS or BH binaries (Orio 2006; Di Stefano et al. 2010). Given that the transient nature of T7 rules out the SNR classification, a variable QSS, associated with a NS or BH X-ray binary, is a rather case for T7.

#### 4.3. Possible Optical Counterparts and Comparison With Magellanic-type Galaxies

The possible optical counterparts of the transient sources were searched in *HST* observations, and we found that the source regions contain multiple optical sources. Without information such as correlated variability, it is hard to identify whether these optical sources are the counterparts or not. Also we note that the counterpart of a post-nova system would be too dim to be detected with the *HST* observations. In any case, the absolute magnitudes, optical colors and X-ray-to-optical flux ratios of the optical sources in the source regions are broadly consistent with those of HMXBs, if we assume one of the optical sources in each error circle as the counterpart. In addition, the absolute magnitudes of the majority of the optical sources identified in our analysis are consistent with the range of Be-HMXBs in SMC (McBride et al. 2008). In the case of SSSs, previous studies suggest that they may have high-mass companions depending on their location in the host galaxy (Di Stefano & Kong 2004; Kuntz et al. 2005), and in the nearby galaxies they are associated with early-type stellar systems (Li et al. 2012; Sturm et al. 2012). Thus we can argue that TSS1 and TSS2 are likely WD X-ray binaries with early-type stellar companion, i.e., WD Be/X-ray binaries, in NGC 4449. However, such Be/WD X-ray binaries are rare and only a few systems (XMMU J052016.0-692505 in LMC, XMMU J010147.5-715550 and MAXI J0158-744 in SMC; Kahabka et al. 2006; Sturm et al. 2012; Li et al. 2012) have been reported in the past. If confirmed, the two transient SSSs would be the first Be/WD X-ray binary systems identified in NGC 4449.

Finally, the Magellanic-type galaxies like LMC, NGC 55 and NGC 4449 have remarkable similarities in their



X-ray properties (see Table 12 of [Stobbart et al. 2006](#)). We further compared the properties of the transient X-ray sources in NGC 4449 with the known transient population of MCs and NGC 55 (see Table 7 of [Jithesh & Wang 2016](#)). Although the number of the transients in NGC 4449 is low, probably not a sufficient sample, the overall properties of the transient X-ray sources (fractions of HMXBs and SSSs, and their luminosities) are consistent with that of the other Magellanic-type galaxies. Our study has further confirmed that the transient X-ray sources in NGC 4449 are also similar to those in MCs and NGC 55.

We thank the anonymous referee for the helpful com-

ments that improved this manuscript. This research has made use of archival data of *Chandra*, *XMM-Newton* and *Swift* observatories through the High Energy Astrophysics Science Archive Research Center (HEASARC) Online Service, provided by NASA Goddard Space Flight Center. VJ acknowledges the financial support from Chinese Academy of Sciences through President's International Fellowship Initiative (CAS PIFI, Grant No. 2015PM059). This research was supported by the Strategic Priority Research Program "The Emergence of Cosmological Structures" of the Chinese Academy of Sciences (Grant No. XDB09000000) and the National Natural Science Foundation of China (11373055). Z.W. acknowledges the support by the CAS/SAFEA International Partnership Program for Creative Research Teams.

## REFERENCES

- Arnaud, K. A. 1996, in *Astronomical Society of the Pacific Conference Series*, Vol. 101, *Astronomical Data Analysis Software and Systems V*, ed. G. H. Jacoby & J. Barnes, 17
- Beuermann, K., Reinsch, K., Barwig, H., et al. 1995, *A&A*, 294
- Burrows, D. N., Hill, J. E., Nousek, J. A., et al. 2005, *SSRv*, 120, 165
- Cash, W. 1979, *ApJ*, 228, 939
- Coe, M. J., Negueruela, I., Buckley, D. A. H., Haigh, N. J., & Laycock, S. G. T. 2001, *MNRAS*, 324, 623
- Di Stefano, R., Kong, A., & Primini, F. A. 2010, *NewAR*, 54, 72
- Di Stefano, R., & Kong, A. K. H. 2003, *ApJ*, 592, 884
- . 2004, *ApJ*, 609, 710
- Fabbiano, G., Kim, D.-W., & Trinchieri, G. 1992, *ApJS*, 80, 531
- Freeman, P. E., Kashyap, V., Rosner, R., & Lamb, D. Q. 2002, *ApJS*, 138, 185
- Gladstone, J., Done, C., & Gierliński, M. 2007, *MNRAS*, 378, 13
- Greiner, J. 2000, *NewA*, 5, 137
- Greiner, J., & Di Stefano, R. 2002, *A&A*, 387, 944
- Greiner, J., Hasinger, G., & Kahabka, P. 1991, *A&A*, 246, L17
- Hachisu, I., Kato, M., & Cassatella, A. 2008, *ApJ*, 687, 1236
- Henze, M., Pietsch, W., Haberl, F., et al. 2010, *A&A*, 523, A89
- Henze, M., Pietsch, W., Haberl, F., et al. 2011, *A&A*, 533, A52
- Henze, M., Pietsch, W., Haberl, F., et al. 2014, *A&A*, 563, A2
- Hickox, R. C., Narayan, R., & Kallman, T. R. 2004, *ApJ*, 614, 881
- Jansen, F., Lumb, D., Altieri, B., et al. 2001, *A&A*, 365, L1
- Jenkins, L. P., Roberts, T. P., Warwick, R. S., Kilgard, R. E., & Ward, M. J. 2005, *MNRAS*, 357, 401
- Jithesh, V., & Wang, Z. 2016, *ApJ*, 821, 24
- Kahabka, P. 1998, *A&A*, 331, 328
- Kahabka, P., & Haberl, F. 2006, *A&A*, 452, 431
- Kahabka, P., Haberl, F., Pakull, M., et al. 2008, *A&A*, 482, 237
- Kahabka, P., Haberl, F., Payne, J. L., & Filipović, M. D. 2006, *A&A*, 458, 285
- Kahabka, P., & Pietsch, W. 1996, *A&A*, 312, 919
- Kahabka, P., & van den Heuvel, E. P. J. 1997, *ARA&A*, 35, 69
- . 2006, *Super-soft sources*, ed. W. H. G. Lewin & M. van der Klis, 461–474
- Kalberla, P. M. W., Burton, W. B., Hartmann, D., et al. 2005, *A&A*, 440, 775
- Karachentsev, I. D., & Drozdovsky, I. O. 1998, *A&AS*, 131, 1
- Kato, M. 2010, *Astronomische Nachrichten*, 331, 140
- Kilgard, R. E., Cowan, J. J., Garcia, M. R., et al. 2005, *ApJS*, 159, 214
- Kong, A. K. H., Di Stefano, R., & Yuan, F. 2004, *ApJL*, 617, L49
- Kuntz, K. D., Gruendl, R. A., Chu, Y.-H., et al. 2005, *ApJL*, 620, L31
- Li, K. L., Kong, A. K. H., Charles, P. A., et al. 2012, *ApJ*, 761, 99
- Liu, J., & Di Stefano, R. 2008, *ApJL*, 674, L73
- Long, K. S., Helfand, D. J., & Grabelsky, D. A. 1981, *ApJ*, 248, 925
- Maccacaro, T., Gioia, I. M., Zamorani, G., et al. 1982, *ApJ*, 253, 504
- McBride, V. A., Coe, M. J., Negueruela, I., Schurch, M. P. E., & McGowan, K. E. 2008, *MNRAS*, 388, 1198
- McGowan, K. E., Coe, M. J., Schurch, M. P. E., et al. 2008, *MNRAS*, 383, 330
- Monet, D. G., Levine, S. E., Canzian, B., et al. 2003, *AJ*, 125, 984
- Ness, J.-U., Schwarz, G., Starrfield, S., et al. 2008, *AJ*, 135, 1328
- Ness, J.-U., Goranskij, V. P., Page, K. L., Osborne, J., & Schwarz, G. 2015, *The Astronomer's Telegram*, 8053,
- Nomoto, K., Saio, H., Kato, M., & Hachisu, I. 2007, *ApJ*, 663, 1269
- Oegelman, H., Beuermann, K., & Krautter, J. 1984, *ApJL*, 287, L31
- Oegelman, H., Orio, M., Krautter, J., & Starrfield, S. 1993, *Nature*, 361, 331
- Orio, M. 2006, *ApJ*, 643, 844
- Ott, J., Walter, F., & Brinks, E. 2005, *MNRAS*, 358, 1423
- Rajolimanana, A. F., Charles, P. A., Meintjes, P. J., Odendaal, A., & Udalski, A. 2013, *MNRAS*, 432, 2886
- Rangelov, B., Prestwich, A. H., & Chandar, R. 2011, *ApJ*, 741, 86
- Reig, P. 2011, *Ap&SS*, 332, 1
- Remillard, R. A., & McClintock, J. E. 2006, *ARA&A*, 44, 49
- Schwarz, G. J., Ness, J.-U., Osborne, J. P., et al. 2011, *ApJS*, 197, 31
- Sequist, E. R., & Bignell, R. C. 1978, *ApJL*, 226, L5
- Shanley, L., Ogelman, H., Gallagher, J. S., Orio, M., & Krautter, J. 1995, *ApJL*, 438, L95
- Starrfield, S., Sparks, W. M., & Truran, J. W. 1974, *ApJS*, 28, 247
- Stobbart, A.-M., Roberts, T. P., & Warwick, R. S. 2006, *MNRAS*, 370, 25
- Stoeke, J. T., Morris, S. L., Gioia, I. M., et al. 1991, *ApJS*, 76, 813
- Strüder, L., Briel, U., Dennerl, K., et al. 2001, *A&A*, 365, L18
- Sturm, R., Haberl, F., Pietsch, W., et al. 2012, *A&A*, 537, A76

- Summers, L. K., Stevens, I. R., Strickland, D. K., & Heckman, T. M. 2003, MNRAS, 342, 690
- Trümper, J., Hasinger, G., Aschenbach, B., et al. 1991, Nature, 349, 579
- Turner, M. J. L., Abbey, A., Arnaud, M., et al. 2001, A&A, 365, L27
- van den Heuvel, E. P. J., Bhattacharya, D., Nomoto, K., & Rappaport, S. A. 1992, A&A, 262, 97
- Vogler, A., & Pietsch, W. 1997, A&A, 319, 459